Chapter 3

Optical Scanning Holography: Principles

Optical scanning holography (OSH) is a form of electronic (or digital) holography. It is a unique, real-time technique where holographic information of a three-dimensional (3-D) object can be acquired by using a single 2-D optical scan. OSH was first implicated by Poon and Korpel when they investigated bipolar incoherent image processing on their acousto-optic heterodyning image processor [1979]. The original idea is later formulated and becomes known as *scanning holography* [Poon (1985)]. The first experimental results were then demonstrated and the technique was eventually called optical scanning holography in order to emphasize the novel fact that holographic recording can be achieved by active optical scanning [Duncan and Poon (1992)]. Thus far, applications of OSH include scanning holographic microscopy [(Poon, Doh, Schilling, Wu, Shinoda, and Suzuki (1995)], 3-D image recognition [(Poon and Kim (1999)], 3-D optical remote sensing [Kim and Poon (1999)], 3-D TV and display [Poon (2002a)], and 3-D cryptography [Poon, Kim, and Doh (2003)]. Scanning holographic microscopy is, by far, the most developed technique that utilizes OSH. Unlike any other holographic microscopes, scanning holographic microscope has a unique property that allows it to take the holographic information of fluorescent specimens in three dimensions. Recently, scientists have been able to achieve better than one-micron resolution in holographic fluorescence microscopy [Indebetouw and Zhong (2006)]. While in chapters 1 and 2, we have covered the necessary backgrounds in mathematics and optics to better understand OSH, in this chapter, we discuss the basic principles of OSH. In chapter 4, we will then discuss some of the previously mentioned applications of OSH in detail. Finally in chapter 5, we will discuss some recent advances in OSH.

3.1 Principle of Optical Scanning

Optical scanning holography involves active *optical scanning* and *optical heterodyning*. In this section, we will discuss the basics of optical scanning. An optical scanner or optical processor scans out a transparency, i.e., information, with an optical beam by moving either the beam or the transparency. A photodetector accepts all light and gives an electrical output

that can either be stored or displayed by some means or another. Hence, optical information will have been converted into electrical information.

Figure 3.1 shows a standard, active optical scanning image processing system. A plane wave (such as the use of a laser in practice) of frequency ω_0, illuminates a pupil function, $p(x,y)$. The complex field emerging from the pupil is then projected through the x-y optical scanner in order to scan over the input object specified by a transparency of $\Gamma_0(x,y)$. The photodetector (PD) then accepts all the light to give out an electrical signal, which contains the processed information for the scanned object. If the scanned electrical signal is digitally stored (i.e., in a computer) in synchronization with the 2-D scan signals of the scanning mechanism (such as the x-y scanning mirrors), what is stored as a 2-D record is then a processed image of the scanned object.

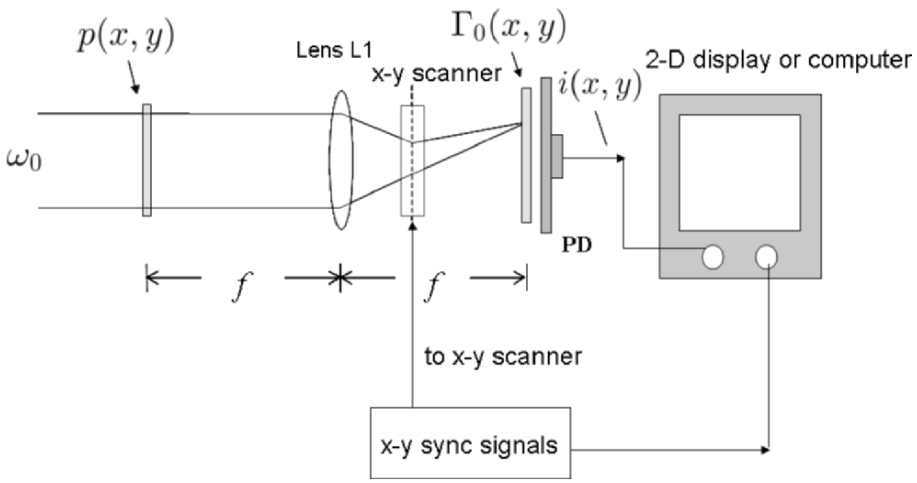

Fig. 3.1 An active optical scanning image processing system.

Let us now discuss photodetection and see how light information can be converted into electrical information. Assume that the photodetector's surface is on the $z=0$ plane and that the incident complex field on the detector's surface is given by $\psi_p(x,y)\exp(j\omega_0 t)$ as shown in Fig. 3.2. Since the photodetector only responds to intensity, i.e., $|\psi_p \exp(j\omega_0 t)|^2$, it gives the current, i, as an output by spatially integrating the intensity over the active area, D, of the detector:

$$i \propto \int_D |\psi_p \exp(j\omega_0 t)|^2 dxdy = \int_D |\psi_p|^2 dxdy. \tag{3.1-1}$$

For example, if the incident field is a plane wave of amplitude A, i.e., $\psi_p = A$, the current output is given by

$$i \propto \int_D |A|^2 dxdy = A^2 D, \tag{3.1-2}$$

which is a constant. However, take for instance that if the light has been intensity-modulated, i.e., $|\psi_p|^2 = m(t)$, where $m(t)$ is the modulating signal, the current will then give an output that varies with the modulation. This is useful for laser communications systems [Pratt (1969)].

Note that since $\psi_p(x,y) = |\psi_p(x,y)|\exp[j\phi(x,y)]$, the output current can only contain the magnitude information, i.e., $|\psi_p|$, and the phase information is completely lost. This type of photodetection is known as *optical direct detection* (or *optical incoherent detection*).

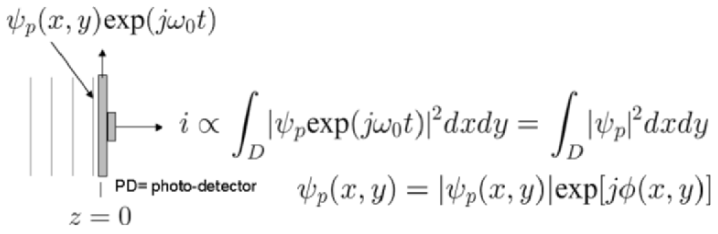

Figure 3.2 Optical direct detection.

Once we comprehend photodetection, we can return to Fig. 3.1 to calculate the current output given after scanning the transparency, $\Gamma_0(x,y)$. Instead of modeling the transparency that is being scanned by an optical beam, as shown by Fig. 3.3, we assume that the transparency, Γ_0, is moving through the optical beam. In Fig. 3.3, the plane of the photodetector is on the $x' - y'$ plane and the optical scanning beam specified by a complex field, $b(x', y')$, is stationary at the origin of the $x' - y'$ plane. By scanning or sampling we mean that successive points (x, y, in transparency coordinates) of Γ_0 are brought into coincidence with the center (x', $y' = 0$) of the optical beam in the $x' - y'$ plane.

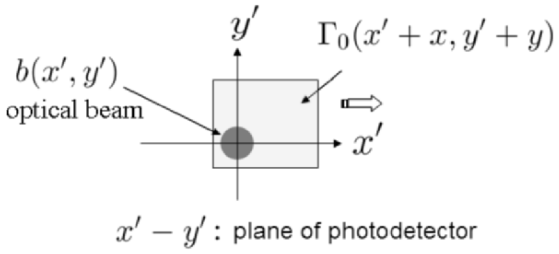

Fig. 3.3 Scanning situation.

In Fig. 3.3, the arguments, x and y, of Γ_0 signify that the transparency is moving or translating with respect to the optical beam. Therefore, the total complex field reaching the photodetector is $b(x', y')\Gamma_0(x' + x, y' + y)$. The photodetector collects all the transmitted light and delivers a current, i. According to Eq. (3.1-1), i is given by

$$i(x, y) \propto \int_D |b(x', y')\ \Gamma_0(x' + x, y' + y)|^2 dx' dy', \tag{3.1-3}$$

where $x = x(t)$ and $y = y(t)$ represent the instantaneous position of the transparency. Alternatively, scanning imaging can be modeled by moving the optical beam across the transparency, which results in the following equation:

$$i(x, y) \propto \int_D |\Gamma_0(x', y')b(x' - x, y' - y)|^2 dx' dy'.$$

If we let $x' - x = x''$ and $y' - y = y''$ and then substitute them into the above equation, we have

$$i(x, y) \propto \int_D |\Gamma_0(x'' + x, y'' + y)b(x'', y'')|^2 dx'' dy'',$$

which is identical to Eq. (3.1-3). We shall use the formulation shown in Eq. (3.1-3) to represent optical scanning throughout the book. Note that for uniform scan speed V, we have $x(t) = Vt$ and $y(t) = Vt$. When we rearrange Eq. (3.1-3), we have

$$\begin{aligned} i(x, y) &\propto \int_D |b(x', y')|^2\ |\Gamma_0(x' + x, y' + y)|^2 dx' dy' \\ &= |b(x, y)|^2 \otimes |\Gamma_0(x, y)|^2. \end{aligned} \tag{3.1-4}$$

Note that this result is interesting because it is an incoherent optical system where only the intensities are processed, i.e., $|\Gamma_0(x, y)|^2$ is processed by $|b(x, y)|^2$ even though the object, $\Gamma_0(x, y)$, originally may be complex in nature. Since the beam complex field, $b(x, y)$, and the pupil, $p(x, y)$, are in the back and the front focal plane of lens L1, respectively, as shown in Fig. 3.1, they are related by a Fourier transformation where [see Eq. (2.4-6)]

$$b(x, y) = \mathcal{F}_{xy}\{p(x, y)\}\Big|_{\substack{k_x = k_0 x/f \\ k_y = k_0 y/f}}. \tag{3.1-5}$$

Figure 3.4 shows a commercially available x-y scanning system from General Scanning™. The mirrors are driven by galvanometers. The figure on

the right is a close-up of the x-y scanning mirrors positioned orthogonally to each other (one direction for the x-scanning and the other for the y-scanning).

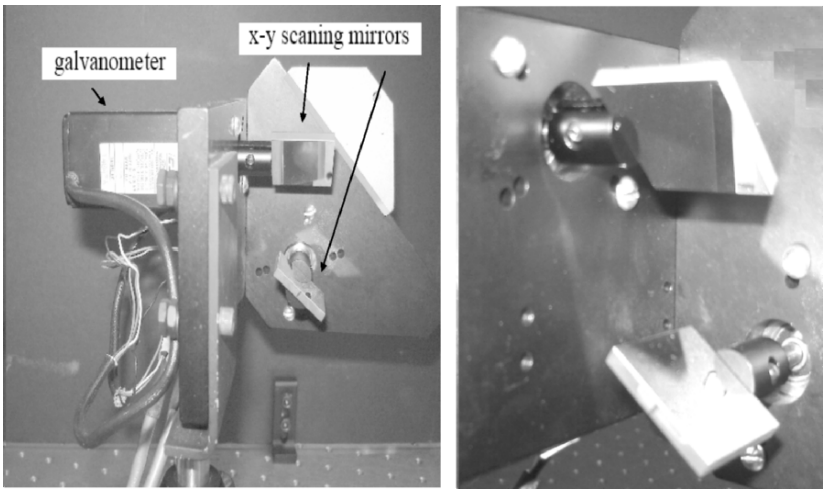

Fig. 3.4 x-y optical scanning system.

3.2 Optical Heterodyning

In the last section, we have shown that a simple optical scanning system that employs optical direct detection cannot extract any phase information of the incident complex field. While holography requires the preservation of the phase information, we, therefore, need to find a way to preserve the phase information during photodetection if we are expected to use optical scanning to record holographic information. The solution to this problem is *optical heterodyning*.

Figure 3.5 shows an optical heterodyne detection. The half-silvered mirror combines two mutually coherent laser beams; the information optical signal beam and the reference optical signal beam, having temporal frequencies of ω_0 and $\omega_0 + \Omega$, respectively [in the next section, we will show how laser beams of different temporal frequencies can be achieved by using acousto-optics]. For simplicity, we will consider the information signal and the reference signal, both as plane waves expressed by $\psi_p \exp(j\omega_0 t)$ and $B\exp[j(\omega_0 + \Omega)t]$ on the surface of the photodetector, respectively. Hence, the total field on the surface of the photodetector is $\psi_t = \psi_p \exp(j\omega_0 t) + B\exp[j(\omega_0 + \Omega)t]$. Since the photodetector only detects intensity, the current output is then given by

$$i \propto \int_D |\psi_t|^2 dx dy$$

$$= \int_D |\psi_p \exp(j\omega_0 t) + B\exp[j(\omega_0 + \Omega)t]|^2 dx\,dy$$

$$= D[A^2 + B^2 + 2AB\cos(\Omega t - \phi)], \tag{3.2-1}$$

where we assume that the information signal is $\psi_p = Ae^{j\phi}$, which has an amplitude of A and phase information, ϕ. Also, for simplicity, we assume that B is real in the above equation. The term, $A^2 + B^2$, is the DC current (or the *baseband current*), whereas the term $AB\cos(\Omega t - \phi)$ is the AC current (or the *heterodyne current*) due to the *mixing* or *heterodyning* of the two optical signals at different frequencies [Poon (2002b), Poon and Kim (2006)]. Also note that the amplitude and the phase of the information signal both have been preserved in the current as it is clearly indicated in the last term of Eq. (3.2-1). Hence, optical heterodyning can preserve the amplitude and phase of the information signal. This type of photodetection is known as *optical heterodyne detection (*or *optical coherent detection*).

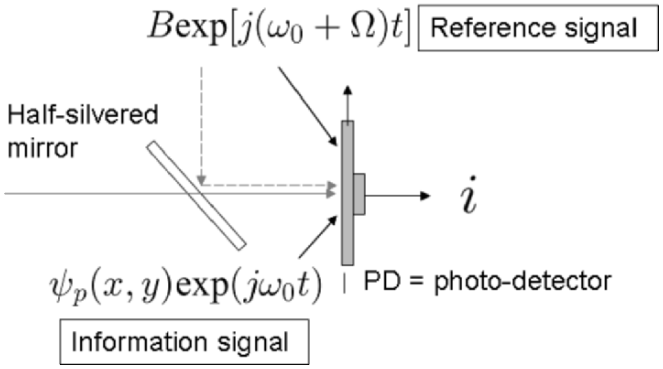

Fig. 3.5 Optical heterodyne detection.

Now that we have shown how the current, i, contains the amplitude and phase information through heterodyning, we will discuss how to extract this information electronically. Figure 3.6 shows an *electronic multiplexing detection*.

The current, i, first passes through a bandpass filter that is tuned to the heterodyne frequency, Ω, in order to reject the baseband current and to extract the heterodyne current, $i_\Omega \propto A\cos(\Omega t - \phi)$. The heterodyne current splits into two channels to obtain two outputs, i_c and i_s, as shown in Fig. 3.6. Each channel actually performs *lock-in detection*, which consists of electronically multiplying the incoming signal with the cosine or sine of the heterodyne frequency, and then using lowpass filtering to extract the phase of the heterodyne current. Let us now see how it is mathematically performed.

First, consider the upper channel where the electronic multiplier gives

$$i_\Omega \times \cos(\Omega t) = A\cos(\Omega t - \phi)\cos(\Omega t)$$

$$= \frac{1}{2}A\cos(-\phi) + \frac{1}{2}A\cos(2\Omega t - \phi) \tag{3.2-2}$$

as output, and where we have used the following trigonometric identity:

$$\cos\alpha\cos\beta = \frac{1}{2}\cos(\alpha - \beta) + \frac{1}{2}\cos(\alpha + \beta).$$

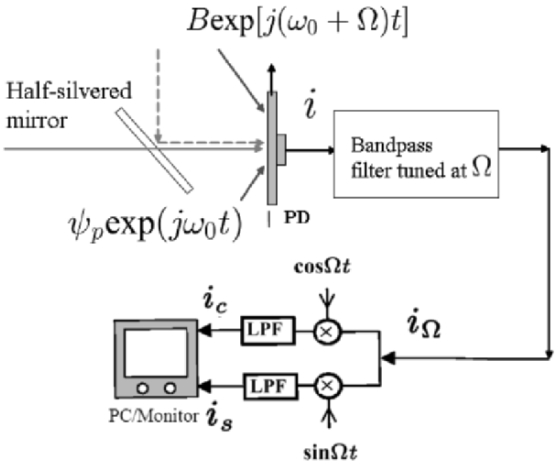

Fig. 3.6 Electronic multiplexing detection.

By using a lowpass filter on the output of the multiplier (which means we are rejecting the frequency of 2Ω), we can obtain the *in-phase component* of the heterodyne current, i_Ω, which is given by

$$i_c = A\cos(\phi). \tag{3.2-3a}$$

Apart from some constant, Eq. (3.2-3a) is really the first term of Eq. (3.2-2). Similarly, the lower channel of Fig. 3.6 gives the *quadrature component* of the heterodyne current, i_Ω, which is given by

$$i_\mathrm{s} = A\sin(\phi), \tag{3.2-3b}$$

where we can use the identity,

$$\cos\alpha\sin\beta = \frac{1}{2}\sin(\alpha + \beta) - \frac{1}{2}\sin(\alpha - \beta),$$

to obtain this result. Now, once i_c and i_s have been extracted and stored in a computer, we can perform the following complex addition:

$$i_c + j\, i_s = A\cos(\phi) + jA\sin(\phi) = A\exp(j\phi). \tag{3.2-4}$$

Note that this result is the full recovery of the information signal, $\psi_p = A e^{j\phi}$, from the photodetector's current given by Eq. (3.2-1). In fact, we will take advantage of optical heterodyning and electronic multiplexing detection by obtaining holographic information without the twin-image noise. We will return to this topic later.

3.3 Acousto-Optic Frequency Shifting

When we employ optical heterodyning as shown in Fig. 3.5, we need to create two laser beams of different temporal frequencies. In this section, we will discuss a common device used for shifting light frequency known as the *acousto-optic frequency shifter* (AOFS) or *acousto-optic modulator* (AOM) [Korpel (1981)].

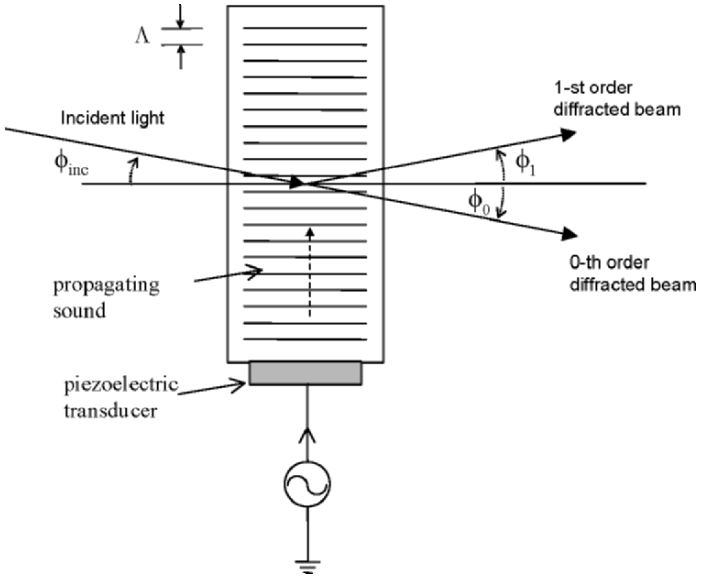

Fig. 3.7 Acousto-optic modulator.

An acousto-optic modulator is a spatial light modulator that consists of an acoustic medium, such as glass, that is bonded to a piezoelectric transducer. When an electrical signal is applied to the transducer, a sound wave propagates through the acoustic medium causing perturbations in the index of refraction, which is proportional to the electrical excitation. This in turn modulates the laser beam that traverses the acoustic medium. Thus, the

acousto-optic modulator, as shown in Figure 3.7, may be thought to act similar to *phase grating* with an effective grating line separation equal to the wavelength, Λ, of the sound in the acoustic medium. As it turns out, for a very specific incident angle, ϕ_{inc}, the sound grating splits incident light into two diffracted beams, namely the 1-st order diffracted beam and the 0-th order diffracted beam at angles ϕ_1 and ϕ_0, respectively. This is shown in Fig. 3.7. We shall identify these angles next.

One of the simplest explanations used to describe the interaction between sound and a laser is to treat the interaction as a collision of particles, namely *photons* and *phonons*. In order for these particles to have well-defined momenta and energies, we must assume that we have an interaction of plane waves of light and sound. In other words, we assume that the width of the transducer is sufficiently wide enough to produce plane wave fronts at a single frequency.

We will now consider two conservation laws that exist during the collison: the *conservation of energy* and the *conservation of momentum*. The condition for conservation of momentum is

$$\hbar\vec{k}_{+1} = \hbar\vec{k}_0 + \hbar\vec{K}\ , \tag{3.3-1}$$

where $\hbar\vec{k}_0$ and $\hbar\vec{K}$ are the momenta of the incident photon and phonon, respectively, and $\hbar\vec{k}_{+1}$ is the momentum of the scattered photon. $\vec{k}_{+1}$, $\vec{k}_0$, and $\vec{K}$ are the corresponding wavevectors of the particles, and $\hbar = h/2\pi$ where h is *Planck's constant*. Now, from the conservation of energy, we have

$$\hbar\omega_{+1} = \hbar\omega_0 + \hbar\Omega, \tag{3.3-2}$$

where $\hbar\omega_{+1}$, $\hbar\omega_0$, and $\hbar\Omega$ are the energies of the scattered photon, incident photon, and phonon, respectively. ω_{+1}, ω_0, and Ω are the corresponding radian frequencies of the particles.

After dividing Eq. (3.3-1) by $\hbar$, we have

$$\vec{k}_{+1} = \vec{k}_0 + \vec{K}\ . \tag{3.3-3}$$

Also, from Eq. (3.3-2), the corresponding conservation of energy takes the form

$$\omega_{+1} = \omega_0\ + \Omega. \tag{3.3-4}$$

Figure 3.8a) shows the wave-vector interaction diagram and is constructed based on Eq. (3.3-3). For all practical cases, $|\vec{K}| \ll |\vec{k}_0|$, the magnitude of $\vec{k}_{+1}$ is essentially equal to that of $\vec{k}_0$, and the wave-vector triangle shown in Fig. 3.8a) is, therefore, nearly isosceles. Note that the closed triangle in Figure 3.8a) stipulates that there are certain critical angles of incidence for the interaction of plane waves of light and sound. The stipulated incident angle, ϕ_{inc}, is called the *Bragg angle*, which is given by

$$\sin(\phi_B) = \frac{K}{2k_0} = \frac{\lambda_0}{2\Lambda}, \tag{3.3-5}$$

where $k_0 = |\vec{k}_0| = 2\pi/\lambda_0$ is the wavenumber of light inside the acoustic medium and λ_0 is the wavelength of light. $K = |\vec{K}| = 2\pi/\Lambda$ is the wavenumber of sound and Λ is the wavelength of sound. Note that the diffracted beams differ in direction by an angle equal to $2\phi_B$ as shown in Fig. 3.8a). $\phi_1$and ϕ_0 in Fig. 3.7 must then be equal to ϕ_B.

Figure 3.8b) shows that the 1-st diffracted beam is being up-shifted in frequency as is required by Eq. (3.3-4). The interaction described by Eq. (3.3-4) is called an *upshifted interaction* because the frequency of the diffracted beam, ω_{+1}, has been upshifted by the amount of the sound frequency, Ω. It is also clear that since we really do have a traveling sound wave, the frequency of the diffracted light is Doppler shifted.

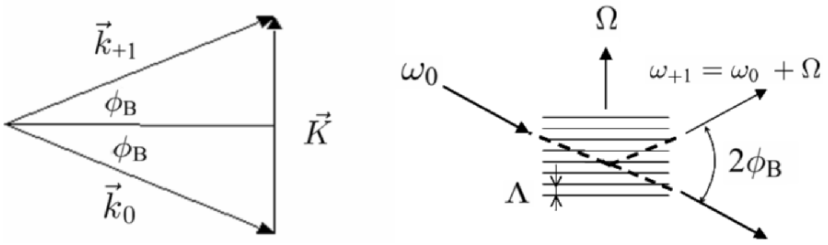

Fig. 3.8 Acousto-optic interaction:
a) wave-vector diagram, b) experimental configuration.

The frequencies of sound waves produced in laboratories range from about 100 KHz to 3 GHz. Figure 3.9 shows a commercially available acousto-optic modulator, Model AOM-40, from IntraAction Corporation. It uses dense flint glass as an acoustic medium (refractive index $n_0 \sim 1.65$) and operates at a sound center frequency of $f_s = 40$ MHz. Therefore, in Fig. 3.9, the sound wave travels in the glass from the left to the right at a velocity of $V_s \sim$4000m/s with a sound wavelength of $\Lambda = V_s/f_s \sim$ 0.1 mm. If a He-Ne laser is used (its wavelength is about $0.6328\mu m$ in air), its wavelength inside the glass is $\lambda_0 \sim 0.6328\mu m/n_0 \sim 0.3743\mu m$. Hence, according to Eq. (3.3-5), the Bragg angle, inside the acoustic medium is $\sim 1.9 \times 10^{-3}$radian or about 0.1 degrees. In Fig. 3.9, we have identified the two diffracted laser spots at the far background. The incident laser beam (not visible to the eye as it traverses across a transparent medium of glass) is traveling through the glass along the long dimension of the piezoelectric transducer.

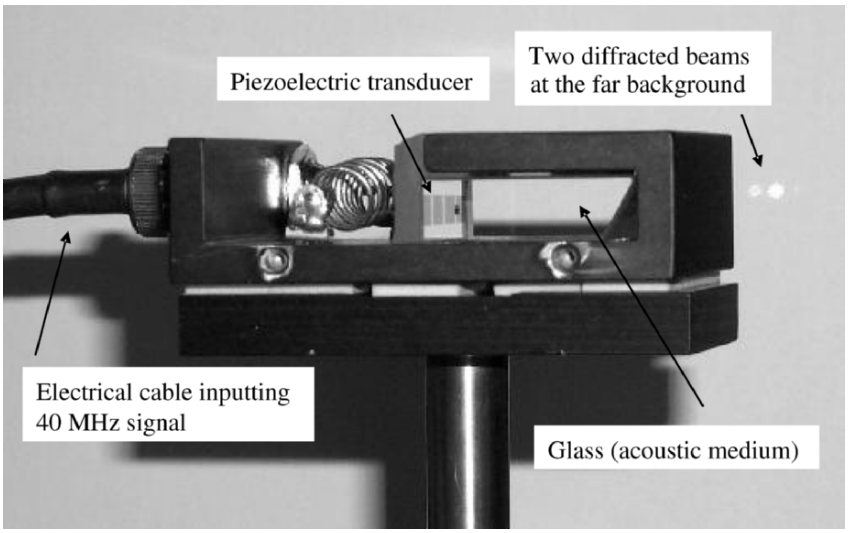

Fig. 3.9 Typical acousto-optic modulator operating at 40 MHz
[Adapted from Poon (2002b)].

3.4 Two-Pupil Optical Heterodyne Scanning Image Processor

We have previously discussed optical scanning and optical heterodyning in prior sections. We have also discussed pupil function in an optical system, and we have shown that the pupil function can modify the characteristics of spatial filtering in an optical system [see Fig. 2.14]. In this section, we are in a position to discuss optical heterodyne scanning from which optical scanning holography is based. Since optical heterodyne scanning requires two optical beams to mix or heterodyne, we must, therefore, have two pupils in the optical system. One can envision that an optical system that has two pupils will have greater processing power because spatial filtering will now be controlled not only by a single pupil, as in conventional optical systems, but by two pupils. These systems are called *two-pupil systems* [Lohmann and Rhodes (1978), Poon and Korpel (1979)]. The article by Indebetouw and Poon provides a review of two-pupil approaches on incoherent image processing [1992].

Figure 3.10 shows a typical two-pupil optical heterodyne scanning image processor, which was originally developed and analyzed by Poon [1985]. We shall develop some mathematical descriptions of this system, which will eventually lead to the concept of optical scanning holography.

Beamsplitters BS and BS_1, and mirrors M and M_1 form the Mach-Zehnder interferometer. The pupil, $p_1(x, y)$, is illuminated by a collimated laser at temporal frequency ω_0. The other pupil, $p_2(x, y)$, is illuminated by the laser of temporal frequency $\omega_0 + \Omega$. The laser's temporal frequency offset by Ω is introduced by an acousto-optic frequency shifter (AOFS) as shown in

the figure. Note that the figure shown in Fig. 3.10 is highly schematic because the details on selecting the first-order diffracted beam, which is the frequency-shifted beam at frequency $\omega_0 + \Omega$, emerging from the AOFS are not shown. The two pupils are located at the front focal planes of lens L_1 and L_2, both with a focal length of f. The two pupils are then combined by the beamsplitter, BS_1, in order to focus the light onto the 2-D, $x - y$ scanning mirrors, which are located on the back focal plane of lenses L_1 and L_2. The combined optical beams are then used to 2-D raster scan over an object of amplitude distribution, $\Gamma_0(x, y; z)$, which is located at a distance of z away from the focal plane of the two lenses. Lens L_3 is used to collect all the transmitted light (or scattered light if the object is diffusely reflecting) onto the photodetector (PD), which gives $i(x, y)$ as its current output. An electronic bandpass filter (BPF) tuned at the heterodyne frequency of Ω provides an output of a scanned and processed current $i_\Omega(x, y)$. We shall further develop the mathematical expression of $i_\Omega(x, y)$.

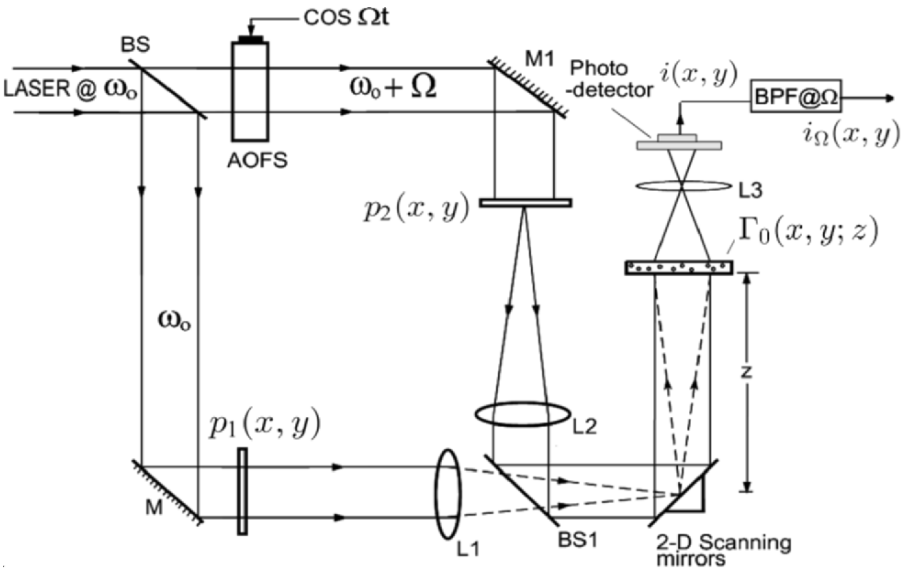

Fig. 3.10 A typical two-pupil optical heterodyne scanning system.

The combined optical scanning complex field, $S(x, y; z)$, located at a distance of z away from the focal plane of the two lenses, is given by

$$S(x, y; z) = P_{1z}(\frac{k_0 x}{f}, \frac{k_0 y}{f}) \exp(j\omega_0 t) + P_{2z}(\frac{k_0 x}{f}, \frac{k_0 y}{f}) \exp[j(\omega_0 + \Omega)t] \,, \tag{3.4-1}$$

where $P_{iz}(\frac{k_0 x}{f},\frac{k_0 y}{f})$ is the field distribution z away from the scanning mirrors and through Fresnel diffraction, is given by

$$P_{iz}(\frac{k_0 x}{f},\frac{k_0 y}{f}) = P_i(\frac{k_0 x}{f},\frac{k_0 y}{f}) * h(x,y;z),\ i=1,2\,. \tag{3.4-2}$$

In Eq. (3.4-2), $P_i(\frac{k_0 x}{f},\frac{k_0 y}{f})$ is the field distribution in the back focal plane of lenses L_1 and L_2, and apart from some inessential constant and a constant phase factor, is given by [see Eq. (2.4-6)]

$$P_i(\frac{k_0 x}{f},\frac{k_0 y}{f}) = \mathcal{F}\{p_i(x,y)\}\Big|_{\substack{k_x=k_0 x/f \\ k_y=k_0 y/f}}\,. \tag{3.4-3}$$

Now, as previously mentioned, the combined optical field or the scanning pattern, given by Eq. (3.4-1), is used to two-dimensionally scan an object with an amplitude transparency of $\Gamma_0(x,y;z)$ located at a distance z from the scanning mirrors. According to the principle established by Eq. (3.1-3) for optical scanning, the photodetector, which responds to the incident intensity of the optical transmitted field or scattered field, generates a current given by

$$i(x,y;z) \propto \int_D |S(x',y';z)\Gamma_0(x'+x,y'+y;z)|^2 dx'dy'$$

$$= \int_D \Big| \Big[P_{1z}(\frac{k_0 x'}{f},\frac{k_0 y'}{f})\ \exp(j\omega_0 t) + P_{2z}(\frac{k_0 x'}{f},\frac{k_0 y'}{f}) \exp[j(\omega_0+\Omega)t] \Big]$$

$$\times\ \Gamma_0(x+x',y+y';z) \Big|^2 dx'dy'. \tag{3.4-4}$$

After a bandpass filter (BPF) is tuned to a frequency of Ω, the heterodyne current from Eq. (3.4-4) becomes

$$i_\Omega(x,y;z) = \mathrm{Re}\Big[\int_D P_{1z}^*(\frac{k_0 x'}{f},\frac{k_0 y'}{f})\ P_{2z}(\frac{k_0 x'}{f},\frac{k_0 y'}{f})$$

$$\times\ |\Gamma_0(x+x',y+y';z)|^2 dx'dy' \exp(j\Omega t) \Big], \tag{3.4-5}$$

where we have adopted the convention for the phasor ψ_p as $\psi(x,y,t) = \mathrm{Re}[\psi_p(x,y,t)\exp(j\Omega t)]$, where Re[.] denotes the real part of the content inside the bracket. Equation (3.4-5) can be written as

$$i_{\Omega}(x,y;z) = \text{Re}[i_{\Omega_p}(x,y;z)\exp(j\Omega t)], \tag{3.4-6a}$$

where

$$i_{\Omega_p}(x,y;z) = \int\int_D P_{1z}^*(\frac{k_0x'}{f},\frac{k_0y'}{f})P_{2z}(\frac{k_0x'}{f},\frac{k_0y'}{f}) \tag{3.4-6b}$$

$$\times\, |\Gamma_0(x+x',y+y';z)|^2dx'dy'$$

is the output phasor containing the amplitude and the phase information of the heterodyne current. The amplitude and the phase information of the current constitute the scanned and the processed version of the object $|\Gamma_0|^2$and from Eq. (3.4-6), we can write

$$i_{\Omega}(x,y;z) = |i_{\Omega_p}(x,y;z)|\cos[(\Omega t + \phi_p(x,y;z)],$$

where $i_{\Omega_p} = |i_{\Omega_p}|\exp(j\phi_p)$. Note that we can re-write Eq. (3.4-6b) in terms of the following correlation:

$$i_{\Omega_p}(x,y;z) = P_{1z}(\frac{k_0x}{f},\frac{k_0y}{f})\, P_{2z}^*(\frac{k_0x}{f},\frac{k_0y}{f}) \otimes |\Gamma_0(x,y;z)|^2. \tag{3.4-7}$$

Similar to conventional optical scanning systems (or incoherent optical systems), only the intensity distribution, i.e., $|\Gamma_0|^2$ will be processed and the optical system is therefore incoherent. However, $|\Gamma_0|^2$ is not strictly processed by an intensity quantity, and as indicated by Eq. (3.4-7) the processing element, $P_{1z}P_{2z}^*$, can be bipolar or even complex, thereby leading to the concept of *complex incoherent image processing*.

Equation (3.4-7) relates the input quantity to the output quantity and from this we can now define the optical transfer function (OTF) of the system to be

$$OTF_{\Omega}(k_x,k_y;z) = \mathcal{F}\{i_{\Omega_p}(x,y;z)\}/\mathcal{F}\{|\Gamma_0(x,y;z)|^2\}. \tag{3.4-8}$$

By taking the Fourier transform of Eq. (3.4-7) and combining its result with Eq. (3.4-8), we obtain the equivalent,

$$OTF_{\Omega}(k_x,k_y;z) = \mathcal{F}^*\{\, P_{1z}(\frac{k_0x}{f},\frac{k_0y}{f})\, P_{2z}^*(\frac{k_0x}{f},\frac{k_0y}{f})\}. \tag{3.4-9}$$

In terms of the pupils p_1 and p_2, we substitute Eqs. (3.4-2) and (3.4-3) into Eq. (3.4-9) to get

$$OTF_{\Omega}(k_x, k_y; z) = \exp[j\frac{z}{2k_0}(k_x^2 + k_y^2)]$$

$$\times \int\int p_1^*(x', y')p_2(x' + \frac{f}{k_0}k_x, y' + \frac{f}{k_0}k_y)\exp[j\frac{z}{f}(x'k_x + y'k_y)]dx'dy'. \tag{3.4-10}$$

This equation was first derived by Poon [1985], and it states that the optical transfer function of the system, OTF_{Ω}, can be modified based on the selection of the two pupils. Now, by using Eq. (3.4-8) and by re-writing Eq. (3.4-6a) in terms of OTF_{Ω}, we obtain

$$\begin{aligned} i_{\Omega}(x, y; z) &= \text{Re}[i_{\Omega_p}(x, y; z)\exp(j\Omega t)] \\ &= \text{Re}[\mathcal{F}^{-1}\{\mathcal{F}\{|\Gamma_0(x, y; z)|^2\}OTF_{\Omega}(k_x, k_y; z)\}\exp(j\Omega t)]. \end{aligned} \tag{3.4-11}$$

By defining the spatial impulse response (or the point spread function) of the optical heterodyne scanning system as

$$h_{\Omega}(x, y; z) = \mathcal{F}^{-1}\{OTF_{\Omega}\}, \tag{3.4-12}$$

we can now re-write Eq. (3.4-11) in the spatial domain as

$$i_{\Omega}(x, y; z) = \text{Re}\Big\{[|\Gamma_0(x, y; z)|^2 * h_{\Omega}(x, y; z)]\exp(j\Omega t)\Big\}. \tag{3.4-13}$$

Equation (3.4-11) or (3.4-13) represents the scanned and processed output current, which is modulated by a temporal carrier at a frequency of Ω. By mixing i_{Ω} with $\cos(\Omega t)$ or $\sin(\Omega t)$, we can demodulate and extract the in-phase component or the quadrature component, respectively. The demodulation system is shown in Fig. 3.6, and the two outputs are given by

$$\begin{aligned} i_c(x, y; z) &= \text{Re}[\mathcal{F}^{-1}\{\mathcal{F}\{|\Gamma_0|^2\}OTF_{\Omega}\}] \quad \text{(frequency domain)} \\ &= \text{Re}[|\Gamma_0|^2 * h_{\Omega}(x, y; z)] \qquad \text{(spatial domain)} \end{aligned} \tag{3.4-14a}$$

and

$$\begin{aligned} i_s(x, y; z) &= \text{Im}[\mathcal{F}^{-1}\{\mathcal{F}\{|\Gamma_0|^2\}OTF_{\Omega}\}] \quad \text{(frequency domain)} \\ &= \text{Im}[|\Gamma_0|^2 * h_{\Omega}(x, y; z)], \qquad \text{(spatial domain)} \end{aligned} \tag{3.4-14b}$$

where Im[.] denotes the imaginary part of the quantity within the bracket. The subscripts "c" and "s" represent the use of $\cos(\Omega t)$ and $\sin(\Omega t)$ respectively, to extract the information from i_{Ω}.

In Eqs. (3.4-14), we have assumed that the input object, $|\Gamma_0(x,y;z)|^2$, is an infinitely thin 2-D object located at a distance of z away from the 2-D scanning mirrors shown in Fig. 3.10. To generalize Eqs. (3.4-14) for 3-D objects, we need to integrate the equations over the depth, i.e., over z, of the 3-D objects. Eqs. (3.4-14) then become [Poon and Kim (1999)]

$$i_c(x,y) = \text{Re}[\int \mathcal{F}^{-1}\{\mathcal{F}\{|\Gamma_0(x,y;z)|^2\}OTF_\Omega\}dz] \tag{3.4-15a}$$

$$= \text{Re}[\int |\Gamma_0(x,y;z)|^2 * h_\Omega(x,y;z)dz] \tag{3.4-15b}$$

and

$$i_s(x,y) = \text{Im}[\int \mathcal{F}^{-1}\{\mathcal{F}\{|\Gamma_0(x,y;z)|^2\}OTF_\Omega\}dz] \tag{3.4-15c}$$

$$= \text{Im}[\int |\Gamma_0(x,y;z)|^2 * h_\Omega(x,y;z)dz]. \tag{3.4-15d}$$

Note that we have left the z-dependence out on the left-hand side of Eqs. (3.4-15) to emphasize that the recorded information is strictly 2-D even for 3-D objects. $i_c(x,y)$ and $i_s(x,y)$ represent the scanned and processed current (or information) of $|\Gamma_0|^2$and can be stored as 2-D records if these currents are stored in synchronization with the signals used to drive the $x-y$ scanning mirrors. Equations (3.4-15) represent the major results of the two-pupil optical heterodyne scanning of a 3-D object. Figure 3.11 shows the overall two-pupil optical heterodyne image processor. The 3-D object is $|\Gamma_0(x,y;z)|^2$, and the final outputs given by Eqs. (3.4-15) are $i_c(x,y)$ and $i_s(x,y)$. Note that while the input object is given by the amplitude distribution, $\Gamma_0(x,y;z)$, the information that can be processed is the intensity distribution given by $|\Gamma_0(x,y;z)|^2$. As it turns out, this is the incoherent mode of operation for the processor, which has so far been inclusively used for various applications such as 3-D fluorescence holographic microscopy, 3-D pattern recognition, optical remote sensing, and 3-D cryptography. In chapter 4, we will further elaborate on some of these applications. In chapter 5, when we consider the advancements towards optical scanning holography, we will describe a coherent mode where the complex distribution of the object can be processed [Indebetouw, Klysubun, Kim, and Poon (2000)]. This can be important when we deal with the phase specimens in biological applications.

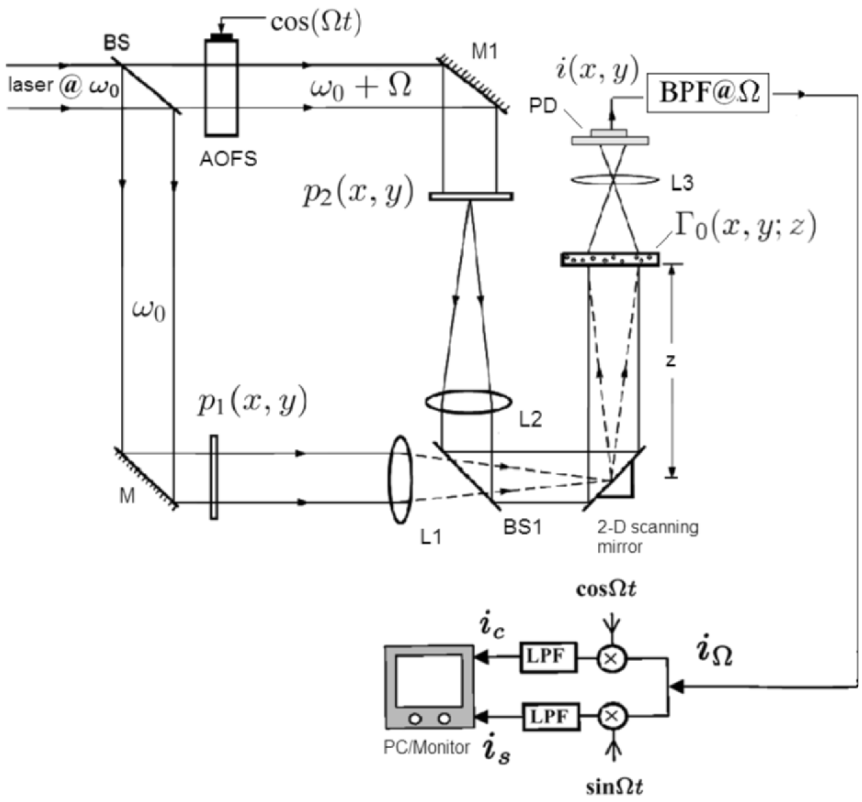

Fig. 3.11 The complete two-pupil optical scanning image processor.

3.5 Scanning Holography

In this section, we will discuss how holographic recording can be accomplished by using the two-pupil optical heterodyne scanning image processor discussed in the last section. The idea was first implicated by Poon and Korpel [1979]. They realized that interesting OTF's can be obtained by drastically modifying one of the pupils in relation to the other. In this context, it is intriguing to realize that there exists a possibility of creating a Fresnel-zone-plate-type impulse response (i.e., its phase is a quadratic function of x and y) in an out-of-focus plane near the focal plane of lenses L1 and L2, i.e., z away from the scanning mirrors shown in Fig. 3.11, by making $p_1(x, y)$ uniform and $p_2(x, y)$ a delta function. When investigating the chirp property, we can determine how far z is from the scanning mirrors, and thus, it carries obvious implication to holographic recording. The original idea, which was later analyzed and called *scanning holography* [Poon (1985)], is to scan the 3-D object in a 2-D raster with a complex

Fresnel-zone-plate-type impulse response created by the interference of a point source and a plane wave emerging from each pupil. A temporal frequency offset is introduced between the two pupils, and the desired signal from a spatially integrating detector is obtained using a heterodyne detection.

Hence, for scanning holography we mathematically let $p_1(x,y)=1$ and $p_2(x,y)=\delta(x,y)$, which are both clearly pictured in Fig. 3.11. With this choice of pupils, according to Eq. (3.4-10), the OTF of the heterodyne scanning system becomes

$$OTF_{\Omega}(k_x,k_y;z)\Big|_{\text{osh}} = \exp[-j\frac{z}{2k_0}(k_x^2+k_y^2)]$$

$$= OTF_{\text{osh}}(k_x,k_y;z), \tag{3.5-1a}$$

and according to Eq. (3.4-12), the corresponding spatial impulse response is

$$h_{\Omega}(x,y;z)\Big|_{\text{osh}} = \frac{-jk_0}{2\pi z}\exp[\frac{jk_0(x^2+y^2)}{2z}]. \tag{3.5-1b}$$

Apart from the constant phase factor, it is interesting to point out that by comparing the spatial frequency transfer function in Fourier optics [see Eq. (2.3-13)] to Eq. (3.5-1a), we have

$$OTF_{\text{osh}}(k_x,k_y;z) = H^*(k_x,k_y;z), \tag{3.5-2a}$$

and similarly in reference to Eq. (2.3-11), we have

$$h_{\Omega}(x,y;z)\Big|_{\text{osh}} = h^*(x,y;z). \tag{3.5-2b}$$

From the result of Eq. (3.5-1b) for scanning holography, apart from some constant, the spatial domain equations, Eqs. (3.4-15b) and (3.4-15d), become

$$i_c(x,y) = \int\Big\{|\Gamma_0(x,y;z)|^2 * \frac{k_0}{2\pi z}\sin[\frac{k_0}{2z}(x^2+y^2)]\Big\}dz$$

$$= H_{\text{sin}}(x,y) \tag{3.5-3a}$$

and

$$i_s(x,y) = \int\Big\{|\Gamma_0(x,y;z)|^2 * \frac{k_0}{2\pi z}\cos[\frac{k_0}{2z}(x^2+y^2)]\Big\}dz \tag{3.5-3b}$$

$$= H_{\text{cos}}(x,y),$$

respectively. What is being two-dimensionally recorded is a hologram. $H_{\sin}(x,y)$ is called the *sine-FZP hologram*, and $H_{\cos}(x,y)$ is the *cosine-FZP hologram* of $|\Gamma_0(x,y;z)|^2$.

To see why Eqs. (3.5-3) correspond to holographic recordings, we will let $|\Gamma_0(x,y;z)|^2 = \delta(x,y)\delta(z-z_0)$, which is a point source located z_0 away from the scanning mirrors. Then Eq. (3.5-3a) becomes

$$H_{\sin}(x,y) = \int \Big\{ \delta(x,y)\delta(z-z_0) * \frac{k_0}{2\pi z} \sin[\frac{k_0}{2z}(x^2+y^2)] \Big\} dz$$

$$= \int \Big\{ \delta(z-z_0) \frac{k_0}{2\pi z} \sin[\frac{k_0}{2z}(x^2+y^2)] \Big\} dz$$

after the 2-D convolution involving x and y. And finally, after the integration along z, the above equation becomes

$$H_{\sin}(x,y) = \frac{k_0}{2\pi z_0} \sin[\frac{k_0}{2z_0}(x^2+y^2)]. \tag{3.5-4a}$$

Note that this is basically the hologram of a point source without the constant bias of A, which appears in Eq. (2.5-4). The constant bias simply gives a zero-order beam upon optical reconstruction. Similarly, Eq. (3.5-3b) gives

$$H_{\cos}(x,y) = \frac{k_0}{2\pi z_0} \cos[\frac{k_0}{2z_0}(x^2+y^2)]. \tag{3.5-4b}$$

In summary, in scanning holography for a single 2-D raster-scan we have two records of the holograms, due to electronic multiplexing detection. Both of the holograms given by Eq. (3.5-3) contain holographic information, but they are not redundant as we will later see that with the two holograms, we can obtain a *twin-image-free* hologram even the recording is made on-axis.

Figure 3.12 shows the very first hologram using scanning holography [Duncan and Poon (1992)]. The hologram is a slit with the size of 50 μm. The term "*optical scanning holography*" was first coined in this article to emphasize that this was the first electronic hologram created by using the active optical scanning technique. To put optical scanning holography into perspective, holograms obtained by scanning techniques at long wavelengths have long been achieved. This has been possible because there is no need to supply a physical reference beam in order to extract holographic information because detectors that are capable of measuring the oscillation of low-frequency radiation (such as acoustic waves or micro-waves) are commonly available, permitting amplitude and phase information to be directly extracted from long wavelength signals.

In general, optical scanning holography (OSH) can be applied to other shorter and longer wavelength systems as long as we can find devices

of that particular wavelength that can generate a collimated beam and a focused beam so that the two beams interfere on the object. In addition, a frequency shifter for that wavelength must be available. In a more futuristic vision, *CO_2 scanning holography* for active optical remote sensing can be possible as 10.6 μm can penetrate the atmosphere with little absorption. At the other end of the light spectrum, *X-ray scanning holography* is becoming a reality because of the increasing existence of X-ray lasers, which should be important if atomic resolution for 3-D specimens is required. In the remainder of the book, we shall use the term *optical scanning holography* or OSH instead of scanning holography.

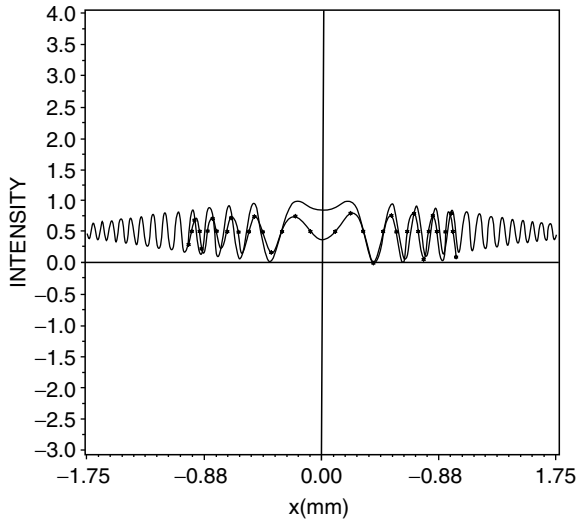

Fig. 3.12 The first hologram obtained using optical scanning holography: solid line: theoretical results; dotted line: experimental results. The object is a 50μm-slit. Reprinted from Duncan and Poon, JOSA A 9, 229 (1992), with permission. © OSA.

The extension of the capabilities of one-dimensional to two-dimensional imaging by using optical scanning holography was subsequently demonstrated by Poon, Doh, Schilling, Wu, Shinoda, and Suzuki [1995]. Fig. 3.13 shows a hologram of a pinhole object. A sine-hologram of the pinhole is shown (this is the well-known FZP). The pinhole is about 50 μm in diameter and approximately 10 cm away from the 2-D scanning mirrors. The plane wave on the pinhole is about 10mm, and comes from a collimated HeNe laser. The spherical wave on the pinhole comes from a focused laser beam of a size of about 3.5 μm. The temporal frequency difference between the plane wave and the spherical wave is 40 MHz. In the same paper mentioned, the authors reported the first 3-D imaging capability using optical scanning holography. Three-dimensional imaging was demonstrated by digitally reconstructing an acquired hologram to show various depths of an image.

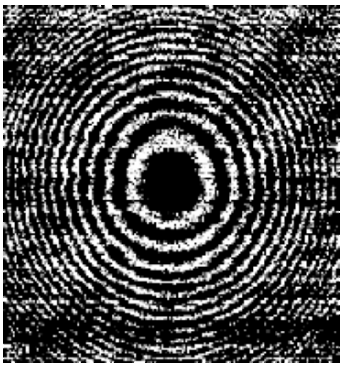

Fig. 3.13 Sine-hologram of a pinhole. The first 3-D imaging capability using OSH is also reported in the paper. Reprinted from T.-C. Poon at al., Optical Engineering 34, 1338, with permission. © 1995 SPIE.

We have discussed the twin-image problem in on-axis holography. And off-axis (or carrier-frequency) holography has been employed to avoid the annoying effect of the twin-image. One of the most popular electronic holographic techniques used to obtain reconstruction free of the twin image is called *phase-shifting holography* [Yamaguchi and Zhang (1997)]. This technique employs phase-shifting on the reference beam to obtain four on-axis holograms in order to calculate the phase of the complex object wave. Using optical scanning holography, we only need to perform a single 2-D scan in order to simultaneously obtain two on-axis holograms - namely the sine-hologram and the cosine-hologram. Since the two holograms can be stored digitally, we can perform a complex addition or subtraction as follows:

$$H_{c\pm}(x,y) = H_{\cos}(x,y) \pm jH_{\sin}(x,y)$$

$$= \int \left\{ |\Gamma_0(x,y;z)|^2 * \frac{k_0}{2\pi z} \exp[\pm j\frac{k_0}{2z}(x^2+y^2)] \right\} dz, \qquad (3.5\text{-}5)$$

where we have used Eqs. (3.5-3a) and (3.5-3b). $H_{c\pm}(x,y)$ is called a *complex Fresnel zone plate hologram*, which contains no twin-image information [Doh, Poon, Wu, Shinoda, and Suzuki (1996)]. To better understand this, we will construct a complex hologram for a point object. Substituting Eqs. (3.5-4a) and (3.5-4b) into Eq. (3.5-5), and apart from some constant, we have

$$H_{c\pm}(x,y) = \exp[\pm \frac{jk_0}{2z_0}(x^2+y^2)]. \qquad (3.5\text{-}6)$$

According to Eqs. (2.5-6b) and (2.5-6c), this hologram can construct either a real point source or a virtual point source, depending on the sign of the argument being chosen in Eq. (3.5-6). For the positive sign in the argument, we will have a real image reconstruction, and for the negative sign, we will have a virtual image reconstruction. In either case, there is no twin-image formation within the complex hologram.

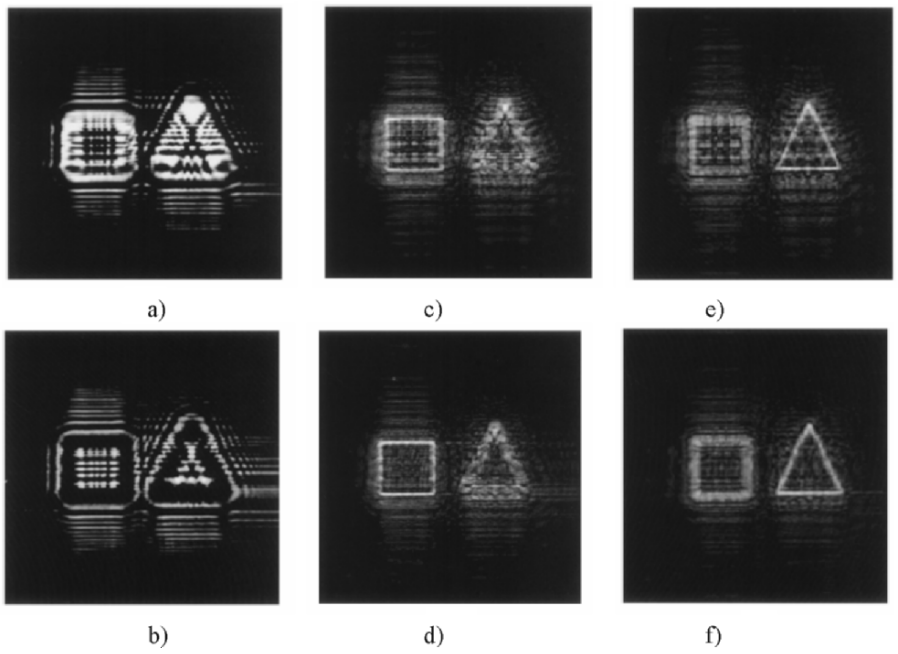

Fig. 3.14 Twin-image elimination with two holograms: a) Cosine-hologram. b) Sine-hologram. c) Reconstruction of a), the cosine-hologram, focused on the square (twin-image noise noticeable). d) Reconstruction of the complex hologram, focused on the square (no twin-image noise). e) Reconstruction of a), focused on the triangle (twin-image noise noticeable). f) Reconstruction of the complex hologram, focused on the triangle (no twin-image noise). Reprinted from Poon et al., Optics Letters 5, 215, (2000), with permission. © OSA.

Figure 3.14 shows the experimental results of eliminating the twin image for three-dimensional images in optical scanning holography. In the experiment, the 3D object consisted of two 35-mm slides that were set up side-by-side and at different distances from the scanning beam. One slide is a square, and the other is a triangle. The depth difference between the two slides is 15-cm. Figure 3.14a) and b) show the cosine- and sine-holograms, respectively. Figure 3.14c) shows the reconstruction of the cosine-hologram. This

reconstruction is focused on the square object but is spoiled by twin-image noise. In Fig. 3.14d), where the complex hologram is used to reconstruct and focus on the square object, twin-image noise is not present. In Fig. 3.14e), the cosine hologram reconstructs an image that is focused on the triangle but spoiled by twin-image noise. In fig. 3.14f), the complex hologram gives a reconstruction without twin-image noise. Thus, the elimination of twin-image in optical scanning holography has been demonstrated using only two holograms. In the demonstration, the use of digital reconstruction has been employed. By using two SLM's (one for the display of a sine-hologram and the other for a cosine-hologram), we can achieve all-optical reconstruction. However, this has yet to be demonstrated optically [Poon (2006)].

Example 3.1 MATLAB Example: Optical Scanning Holography

By substituting the OTF of optical scanning holography, given by Eq. (3.5-1a), into Eqs. (3.4-15a) and (3.4-15c), the sine-hologram and the cosine-hologram will be expressed in terms of spatial frequencies. Therefore, we have

$$i_c(x,y) = \text{Re}[\int \mathcal{F}^{-1}\{\mathcal{F}\{|\Gamma_0(x,y;z)|^2\}OTF_{\text{osh}}(k_x,k_y;z)\}dz]$$

$$= H_{\text{sin}}(x,y) \tag{3.5-7a}$$

and

$$i_{\text{s}}(x,y) = \text{Im}[\int \mathcal{F}^{-1}\{\mathcal{F}\{|\Gamma_0(x,y;z)|^2\}OTF_{\text{osh}}(k_x,k_y;z)\}dz]$$

$$= H_{\text{cos}}(x,y), \tag{3.5-7b}$$

where $OTF_{\text{osh}}(k_x,k_y;z) = \exp[-j\frac{z}{2k_0}(k_x^2 + k_y^2)]$. For this example, we are assuming a planar object to be at a distance of z_0 away from the x-y scanning mirrors, i.e., $|\Gamma_0(x,y;z)|^2 = I(x,y)\delta(z-z_0)$, where $I(x,y)$ is the planar intensity distribution shown in Fig. 3.15a). For the planar intensity object, after integrating over z, Eqs. (3.5-7a) and (3.5-7b) become

$$H_{\text{sin}}(x,y) = \text{Re}[\mathcal{F}^{-1}\{\mathcal{F}\{I(x,y)\}OTF_{\text{osh}}(k_x,k_y;z_0)\}] \tag{3.5-8a}$$

and

$$H_{\text{cos}}(x,y) = \text{Im}[\mathcal{F}^{-1}\{\mathcal{F}\{I(x,y)\}OTF_{\text{osh}}(k_x,k_y;z_0)\}], \tag{3.5-8b}$$

respectively. The above holograms are simulated and shown in Fig. 3.15b) and Fig. 3.15c), respectively where sigma $= z_0/2k_0 = 2.0$ in OSH.m listed in Table 3.1. We can also construct a complex FZP hologram by using Eq. (3.5-5):

$$H_{c+}(x,y) = H_{\cos}(x,y) + jH_{\sin}(x,y)$$

$$= \mathcal{F}^{-1}\{\mathcal{F}\{I(x,y)\}OTF_{\text{osh}}(k_x,k_y;z_0)\}. \qquad (3.5\text{-}9)$$

For digital reconstruction, we will simply convolve the above holograms with the spatial impulse response in order to simulate Fresnel diffraction for a distance of z_0. To obtain real image reconstruction formed in front of the hologram, we will use the following equation:

$$H_{\text{any}}(x,y)*h(x,y;z_0),$$

where $H_{\text{any}}(x,y)$ represents any one of the above holograms, i.e., the sine-hologram, the cosine-hologram or the complex hologram. In OSH.m, the above equation is implemented in the Fourier domain using the following equation [see Eqs. (1.2-3a) and (1.2-3b)]:

Reconstructed real image

$$\propto \mathcal{F}^{-1}\{\mathcal{F}\{H_{\text{any}}(x,y)\}H(k_x,k_y;z_0)\}$$

$$= \mathcal{F}^{-1}\{\mathcal{F}\{H_{\text{any}}(x,y)\}OTF_{\text{osh}}{}^{*}(k_x,k_y;z_0)\}, \qquad (3.5\text{-}10)$$

where we have used Eq. (3.5-2a) to relate OTF_{osh} with the spatial frequency response, $H(k_x,k_y;z_0)$, to obtain the last step. Figures 3.15d), e) and f) show the reconstruction of the sine-hologram, the cosine-hologram, and the complex hologram, respectively.

Note that if the complex hologram is constructed as

$$H_{c-}(x,y) = H_{\cos}(x,y) - jH_{\sin}(x,y),$$

then it will have a reconstructed virtual image that is located at a distance of z_0 behind the hologram. However, if we perform

$$H_{c-}(x,y)*h(x,y;z_0)$$

for reconstruction, we will see a severely out-of-focus image formed at $z = z_0$ as shown in Fig. (3.15g), which is equivalent to the Fresnel diffraction pattern of the original object at a distance of $z = 2z_0$.

a) Original Image, $I(x, y)$.

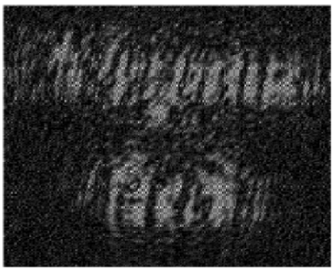

b) Sine-hologram of a).

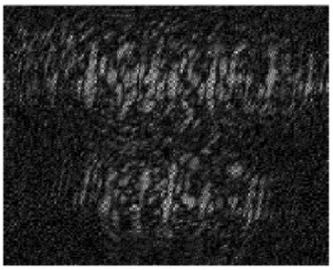

c) Cosine-hologram of a).

d) Reconstruction of sine-hologram.

e) Reconstruction of cosine-hologram.

f) Reconstruction of complex hologram, $H_{c+}(x, y)@z = z_0$.

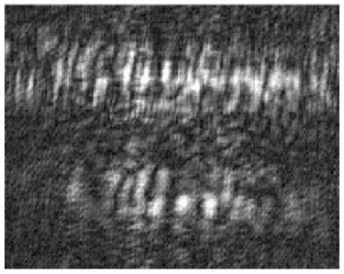

g) Reconstruction of complex hologram, $H_{c-}(x, y)@z = z_0$.

Fig. 3.15 Simulation results using OSH.m.

Table 3.1 OSH.m : m-file for illustrating optical scanning holography.

```
% OSH.m
% Adapted from "Contemporary Optical Image Processing with MATLAB,"
% by Ting-Chung Poon and Partha Banerjee, Table 7.2,
% Pages 222-223, Elsevier (2001).

clear all,
%%Reading input bitmap file
I=imread('vatech.bmp','bmp');
I=I(:,:,1);
figure(1)%displaying input
colormap(gray(255));
image(I)
title('Original image')
axis off
pause

%%Creating OTFosh with SIGMA=z/2*k0 (Eq.(3.5-1a))
ROWS=256;
COLS=256;
sigma=2.0; %not necessary to scale
%kx,ky are spatial frequencies
ky=-12.8;
for r=1:COLS,
  kx=-12.8;
  for c=1:ROWS,
      OTFosh(r,c)=exp(-j*sigma*kx*kx-j*sigma*ky*ky);
      kx=kx+.1;
      end
  ky=ky+.1;
end
max1=max(OTFosh);
max2=max(max1);
scale=1.0/max2;
OTFosh=OTFosh.*scale;

%Recording hologram
% Taking Fourier transform of I
FI=fft2(I);
FI=fftshift(FI);
max1=max(FI);
max2=max(max1);
scale=1.0/max2;
FI=FI.*scale;
% FH is the recorded hologram in Fourier domain
FH=FI.*OTFosh;
H=ifft2(FH);
max1=max(H);
max2=max(max1);
scale=1.0/max2;
```

```
H=H.*scale;
figure(1)
colormap(gray(255));
%Displaying the real part becomes sine-FZP hologram
% Eq. (3.5-8a)
image(2.5*real(256*H));
title('Sine-FZP hologram')
axis off
figure(2)
colormap(gray(255));
%Displaying the imaginary part becomes cosine-FZP hologram
% Eq. (3.5-8b)
image(2.5*imag(256*H));
title('Cosine-FZP hologram')
axis off
%Reconstructing holograms
%Reconstruction of sine-hologram,twin-image noise exists
figure(3)
colormap(gray(255))
H=ifft2(FH);
FRSINEH=fft2(real(H)).*conj(OTFosh); %Eq. (2.5-10)
RSINEH=ifft2(FRSINEH);
image(256*abs(RSINEH)/max(max(abs(RSINEH))))
title('Reconstruction of sine-FZP hologram')
axis off
%FH=FHI;
%Reconstruction with cosine-hologram, twin-image noise exists
figure(4)
colormap(gray(255))
FRCOSINEH=fft2(imag(H)).*conj(OTFosh);
RCOSINEH=ifft2(FRCOSINEH); %Eq. (3.5-10)
image(256*abs(RCOSINEH)/max(max(abs(RCOSINEH))))
title('Reconstruction of cosine-FZP hologram')
axis off

figure(5)
colormap(gray(255))
FRCOMPLEXH=fft2(real(H)+j*imag(H)).*conj(OTFosh);
RCOMPLEX=ifft2(FRCOMPLEXH);
image(1.4*256*abs(RCOMPLEX)/max(max(abs(RCOMPLEX))))
title('Real image reconstruction of complex FZP hologram,Hc+')
axis off

figure(6)
colormap(gray(255))
FRCOMPLEXH2=fft2(real(H)-j*imag(H)).*conj(OTFosh);
RCOMPLEX2=ifft2(FRCOMPLEXH2);
image(1.4*256*abs(RCOMPLEX2)/max(max(abs(RCOMPLEX2))))
title('Reconstruction of complex FZP hologram, Hc-')
axis off
```

3.6 Physical Intuition to Optical Scanning Holography

While we have devoted the last section to developing optical scanning holography from a mathematical point of view, in this section we will be describing optical scanning holography from a physical point of view. Again, to accomplish optical scanning holography, we select $p_1(x,y)=1$ and $p_2(x,y)=\delta(x,y)$ in the two-pupil heterodyne image processor (the situation is shown in Fig. 3.10 clearly) where lens L1 forms a point source and lens L2 forms a plane wave on the scanning mirrors. At a distance of $z=z_0$ away from the scanning mirrors, where the object, $|\Gamma_0(x,y;z)|^2=I(x,y)\,\delta(z-z_0)$, is located, we have an interference between a plane wave and a spherical wave of different temporal frequencies. Hence, the scanning beam intensity is

$$
\begin{aligned}
&I_{\text{scan}}(x,y;t)\\
&=|\,a\exp[j(\omega_0+\Omega)t]\,+\frac{jk_0}{2\pi z_0}\exp[-\frac{jk_0(x^2+y^2)}{2z_0}]\exp(j\omega_0 t)|^2\\
&=\,A+\,B\sin[\frac{k_0}{2z_0}(x^2+y^2)+\Omega t]\\
&=\mathit{TDFZP}(x,y;z_0,t),
\end{aligned}
\tag{3.6-1}
$$

where we have assumed that the plane wave is of amplitude a, and A and B have been defined in Eq. (2.5-3). Note that this equation is basically the same form as that of Eq. (2.5-4) for the recording of an on-axis point source except for the time variable, t. We shall call this a *time-dependent Fresnel zone plate* (TDFZP), which is used to scan over the object in a raster fashion. For a pinhole object, i.e., $I(x,y)=\delta(x,y)$, the photodetector's current, $i(x,y)$, is clearly given by $\mathit{TDFZP}(x,y;z_0,t)$ as the pinhole samples the intensity pattern, which then gives the intensity pattern as output. We can also see mathematically that if we make use of Eq. (3.1-4), we can obtain

$$
\begin{aligned}
i(x,y)&\sim \mathit{TDFZP}(x,y;z_0,t)\otimes\delta(x,y)\\
&=\mathit{TDFZP}(x,y;z_0,t)\\
&=\,A+\,B\sin[\frac{k_0}{2z_0}(x^2+y^2)+\Omega t].
\end{aligned}
$$

After bandpass filtering at Ω, the heterodyne current becomes

$$i_\Omega(x,y) \sim \sin[\frac{k_0}{2z_0}(x^2+y^2)+\Omega t], \tag{3.6-2}$$

and after electronic detection, i.e., multiplying with, say $\cos(\Omega t)$, and lowpass filtering, we obtain

$$i_c(x,y) \sim \sin[\frac{k_0}{2z_0}(x^2+y^2)], \tag{3.6-3}$$

which is again Eq. (3.5-4a). So we can see that optical scanning holography is simply accomplished by raster-scanning a TDFZP over a 3-D object in order to obtain two holograms. The physical situation is shown in Fig. 3.16, where in the pupil plane, we have a point source and a plane wave. In the figure, we show the pattern of the scanning beam on the object slice for a fixed time, say, at $t = t_0 = 0$, which becomes a "static" Fresnel zone plate (FZP). If we let the time run in Eq. (3.6-1), we will physically have running fringes that will be moving toward the center of the zone pattern. Hence, the basic principle of OSH is to simply use the TDFZP to 2-D scan a 3-D object to obtain holographic information for the scanned object. The m-file presented in Table 3.2 will allow us to generate a TDFZP and illustrate the running of fringes.

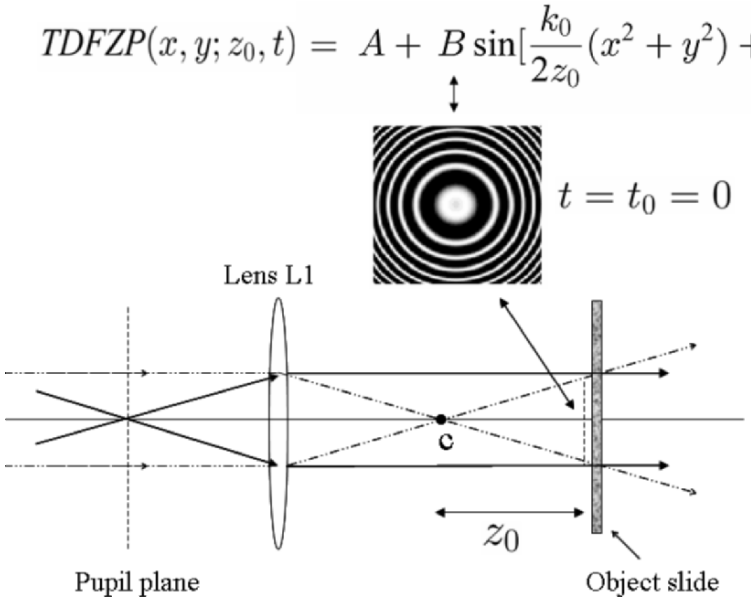

Fig. 3.16 Principle of OSH: use of time-dependent Fresnel zone plate to scan over an object. Adapted from T. -C. Poon, Journal of Holography and Speckle 1, 6-25, (2004).

We can also select the pupils differently to achieve optical scanning holography as long as we can create a time-dependent FZP to scan the 3-D object. For example, we can select $p_1(x,y)=\delta(x,y)$ and $p_2(x,y)=1$ instead of $p_1(x,y)=1$ and $p_2(x,y)=\delta(x,y)$ as we had previously discussed in the two-pupil heterodyne image processor. Then, the scanning intensity become

$$
\begin{aligned}
&I_{\text{scan}}(x,y;t)\\
&=|\,a\exp(j\omega_0 t)+\frac{jk_0}{2\pi z_0}\exp[-\frac{jk_0(x^2+y^2)}{2z_0}]\exp[j(\omega_0+\Omega)t]\,|^2\\
&=A+B\sin[\frac{k_0}{2z_0}(x^2+y^2)-\Omega t]\\
&=TDFZP(x,y;z_0,-t). \qquad (3.6\text{-}4)
\end{aligned}
$$

This will give fringes running away from the center of the zone, and this can be verified by changing the sign in front of B in the expression of FZP(ii,jj,kk) in the TDFZP.m file. As it turns out, this scanning beam gives the same expression for the sine-hologram given by Eq. (3.5-3a). However, the expression for the cosine-hologram is different with a "negative" sign in front of it. Note that the errors and sensitivities produced by the heterodyne method, as well as the impact created by these errors, will not be discussed in this book. Readers should refer to Section 5.4 of the *Handbook of Holographic Interferometry* [Kreis, 2005], which will provide insight into the practical limitations of heterodyning holographic interferometry.

When Ω is set to zero, we have *homodyning* and the time-dependent Fresnel zone plate becomes static. Now by introducing phase shifts between the two interfering waves that are used to generate the Fresnel zone plate, one can obtain three holograms (as a result of three different phase shifts) to alternatively solve the twin-image problem in optical scanning holography [Rosen, Indebetouw and Brooker (2006)].

Table 3.2 TDFZP.m : m-file for illustrating running fringes in TDFZP.

```
% TDFZP.m
% Illustration of running fringes in TDFZP
% The author thanks Kelly Dobson for her initial programming

clear;
B=10.01*10^6;  %temporal frequency, arbitrary
D=6; %Scale arbitrary

t=linspace(0,1,35);
x=linspace(-2.5,2.5,256);
y=linspace(-2.5,2.5,256);
```

```
for ii=1:length(x)
 for jj=1:length(y)
  for kk=1:length(t)
  FZP(ii,jj,kk)=(1+sin(D*(x(ii)^2+y(jj)^2)+B*t(kk))); %TDFZP
  end
 end
end

for ll=1:length(t)
   max1=max(FZP(:,:,ll));
   max2=max(max1);
   scale=1/max2;
   FZP(:,:,ll)=FZP(:,:,ll).*scale;
figure(ll);
colormap(gray(256));
image(256*FZP(:,:,ll));
axis off
F(ll)=getframe;
end

movie(F,10)
```

References

3.1 Duncan, B.D. and T.-C. Poon (1992). "Gaussian beam analysis of optical scanning holography," *Journal of the Optical Society of America A* 9, 229-236.

3.2 Doh, K., T.-C. Poon, M. Wu, K. Shinoda, and Y. Suzuki (1996). "Twin-image elimination in optical scanning holography, " *Laser & Optics Technology* 28, 135-141.

3.3 General Scanning. http://www.gsig.com/scanners/

3.4 Indebetouw, G. and T.-C. Poon (1992). "Novel approaches of incoherent image processing with emphasis on scanning methods," *Optical Engineering* 31, 2159-2167.

3.5 Indebetouw, G., P. Klysubun, T. Kim, and T.-C. Poon (2000). "Imaging properties of scanning holographic microscopy," *Journal of the Optical Society of America A* 17, 380-390.

3.6 Indebetouw, G and W. Zhong (2006). "Scanning holographic microscopy of three-dimensional fluorescent specimens," *Journal of the Optical Society of America A*. 23, 1699-1707.

3.7 IntraAction Corp. http://www.intraaction.com/

3.8 Kim, T and T.-C. Poon (1999). "Extraction of 3-D location of matched 3-D object using power fringe-adjusted filtering and Wigner analysis," *Optical Engineering* 38, 2176-2183.

3.9 Korpel, A. (1981). "Acousto-optics-a review of fundamentals," *Proceedings of the IEEE* 69, 48-53.

3.10 Kreis, T. (2005). *Handbook of Holographic Interferometry*. Wiley-VCH GmbH & Co. KGaA, Weinheim.

3.11 Lohmann, A. W. and W. T. Rhodes (1978). "Two-pupil synthesis of optical transfer functions," *Applied Optics* 17, 1141-1150.

3.12 Poon, T.-C. (1985). "Scanning holography and two-dimensional image processing by acousto-optic two-pupil synthesis," *Journal of the Optical Society of America A* 4, 521-527

3.13 Poon, T.-C. (2002a). "Three-dimensional television using optical scanning holography," *Journal of Information Display* 3, 12-16.

3.14 Poon, T.-C. (2002b). "Acousto-Optics," *Encyclopedia of Physical Science and Technology*, Academic Press.

3.15 Poon, T.-C. (2004). "Recent progress in optical scanning holography," *Journal of Holography and Speckle* 1, 6-25.

3.16 Poon, T.-C. (2006). "Horizontal-parallax-only optical scanning holography," in chapter 10 of *Digital Holography and Three-Dimensional Display: Principles and Applications*, T.-C. Poon ed., Springer, New York, USA.

3.17 Poon, T.-C. and A. Korpel. (1979). "Optical transfer function of an acousto-optic heterodyning image processor," *Optics Letters* 4, 317-319.

3.18 Poon, T.-C., K. Doh, B. Schilling, M. Wu, K. Shinoda, and Y. Suzuki (1995). "Three-dimensional microscopy by optical scanning holography," *Optical Engineering* 34, 1338–1344.

3.19 Poon, T.-C. and T. Kim (1999). "Optical image recognition of three-dimensional objects," *Applied Optics* 38, 370-381.

3.20 Poon, T.-C., T. Kim, G. Indebetouw, B. W. Schilling, M. H. Wu, K. Shinoda, and Y. Suzuki (2000). "Twin-image elimination experiments for three-dimensional images in optical scanning holography," *Optics Letters* 25, 215-217.

3.21 Poon T.-C. and P. P. Banerjee (2001). *Contemporary Optical Image Processing with MATLAB®*. Elsevier, Oxford, UK.

3.22 Poon, T.-C., T. Kim and K. Doh (2003) "Optical scanning cryptography for secure wireless transmission," *Applied Optics* 42, 6496-6503.

3.23 Poon, T.-C. and T. Kim (2006). *Engineering Optics with MATLAB®*. World Scientific Publishing Co., Singapore.

3.24 Pratt, W.K. (1969). *Laser Communications Systems*, John Wiley & Sons.

3.25 Rosen, J., G. Indebetouw, and G. Brooker. "Homodyne scanning holography," *Optics Express* 14, 4280-4285.

3.26 Yamaguchi, I. and T. Zhang (1997). "Phase-shifting digital holography," *Optics Letters* 22, 1268-1270.